Korean J. Chem. Eng., 40(1), 185-194 (2023)
DOI: 10.1007/s11814-022-1266-1

pISSN: 0256-1115
eISSN: 1975-7220

Polyether sulfone-graphite nanocomposite for nanofiltration membrane with enhanced separation, antifouling and antibacterial properties

Sayed Mohsen Hosseini*,†, Sima Mohammadianfar*, Samaneh Koudzari Farahani*, and Sadra Solhi**

*Department of Chemical Engineering, Faculty of Engineering, Arak University, Arak 38156-8-8349, Iran
**School of Medicine, Arak University of Medical Sciences, Arak, Iran
(*Received 15 April 2022 • Revised 10 August 2022 • Accepted 17 August 2022*)

Abstract−Mixed matrix polyether sulfone based-graphite nanoparticle nanofiltration membranes were prepared by phase inversion technique. SEM, SOM, 3D surface analysis, water content, water contact angle, tensile strength, salt rejection, water flux, porosity, antifouling measurements as well as antibacterial activity were used in membrane characterization. SOM images showed graphite nanoparticle distribution in the structure of membranes relatively. The cross section SEM showed that incorporation of graphite nanoparticles into the casting solution had significant effect on the appearance structural properties of the membrane. The water flux of modified membranes was higher than the amount for unmodified membrane obviously. Salt rejection also increased from 82% for unmodified membrane to 91.79% for the membrane containing 0.5 wt% graphite nanoparticles. The water content and porosity increased at 0.05 wt% and 0.5 wt% concentration of graphite nanoparticle, and showed decreasing manner at 0.1 wt% and 1 wt% additives ratios. Utilizing 0.05 wt% G-nanoparticles into the polymeric solution made a membrane with smoother and hydrophilic surface that tended to improved anti-fouling properties. The 0.05 wt% G-nanoparticles/PES membrane showed more suitable behavior than other membranes. Moreover, blended membranes showed antibacterial activity against E-coli.

Keywords: Mixed Matrix Membrane, Nanofiltration, Graphite Nanoparticles, Separation Properties, Antifouling Ability, Antibacterial Activity

INTRODUCTION

Water is a vital source for all living organisms, but unfortunately, water pollution has increased dramatically in recent years due to the development of industries and the increasing population of the world and the misuse of water resources. So that water purification and drinking water supply has become one of the most important problems of the human race. To solve this problem, researchers have studied various ways to reuse waste water. Today membrane technology is widely used in the water treatment industry due to its simplicity of operation, low environmental impact and low maintenance and exploitation costs on a large scale. Among them pressure driven processes, such as microfiltration, ultrafiltration, nanofiltration and reverse osmosis, are widely used in various industries. For example, nanofiltration membranes are more common in water treatment [1-3]. In the nanofiltration process, polymeric membranes are mainly used. Polymeric membranes are highly regarded because of their ease of manufacture, easy modifiability and versatility in material selection. But the limitation of using polymeric membranes is fouling. In fact, this phenomenon reduces the membrane's efficiency and life time. Thus, one of the challenges facing polymeric membranes is the increased antifouling property of membrane. The antifouling property is actually directly related to the surface roughness and the hydrophilicity of the membrane. In the higher hydrophilic properties of the membrane, more water molecules are absorbed at the membrane surface and the undesirable particles are washed from the membrane surface by water flows. On the other hand, it has been observed in various studies that membranes with less roughness and a smoother surface have more antifouling properties. Because at rough surfaces, foulant particles are trapped in the roughness of membrane surface and have a negative effect on membrane performance [4-6]. One of the polymers used in water treatment processes is polyether sulfone (PES). This polymer is known for its high mechanical, chemical, and thermal resistance, but due to its hydrophobic nature, it is inevitably exposed to fouling phenomenon [7-13]. To overcome this limitation, various methods are used to modify the structure and improve membrane performance. One of the methods is to add nanoparticles such as metal nanoparticles (Ag, Pd, many more), metal oxide nanoparticles, metal organic frameworks (ZIF, UIO-66, etc.) and carbon-based nanoparticles (G, GO, MWCNT, etc.). Carbon based nanoparticles due to their good mechanical properties, outstanding electron transfer, high surface area and proper compatibility with polymer matrix have received special attention and much research has been done into the different applications of these materials [14-20].

A nanocarbon-based FO membrane with reduced graphene oxide (RGO) on a carbon nanotube hollow fiber via chemical reduction processes was fabricated by Fan and coworkers. High water permeability and ion selectivity were observed for the RGO active layer and the CNT hollow fiber substrate could weaken the internal concentration polarization, with high porosity and good wettability. The prepared RGO/CNT showed a high water flux, which is 3.3

†To whom correspondence should be addressed.
E-mail: s-hosseini@araku.ac.ir

times more than the commercial membrane [21].

Also, Gholami et al. examined thin-film nanocomposite nanofiltration membranes, which were fabricated by blending aromatic amine-functionalized MWCNTs and aliphatic amine-functionalized MWCNTs. The performance of membranes on the rejection of $NH_4^+HAsO_4^{-2}$, and NO_3^- from polluted groundwater was studied. The aromatic amine-functionalized MWCNTs (AAF-MWCNT) proved that increasing of water permeate flux and arsenic rejection was 15% more than the commercial semi-aromatic polyamide nanofiltration membranes [22].

Li and colleagues, prepared an anion exchange membrane by electro-deposition of graphene oxide (GO) and polydopamine (PDA) coating to improve antifouling performance. The desalination rate, antifouling ability, stability and hydrophilicity of membranes were increased after PDA coating. In addition, PDA coating helped to reduce the roughness of membrane surface [23]. Yang et al. produced novel poly vinyl alcohol (PVA) based mixed matrix membranes fabricated by multiwalled carbon nanotubes (MWCNTs) or carboxylic multiwalled carbon nanotubes (C-MWCNTs) via interfacial adhesion, hydrogen bonding or covalent bonding. Also, when the feed was NaCl solution (35,000 ppm) the overall best performance of salt rejection (99.91%) and water flux (6.96 kg/m^{2}h) was obtained by the PVA/C-MWCNT/MA membrane [24]. The high flux separation of a water-in-oil emulsion by carbon-silica composite nanofiber membranes was investigated by Tai et al. The results showed these membranes have proper flux in separating water from oil under low pressure [25]. Liua et al. studied a UF membrane for water purification. A different model of carbon nanofiber (CNF) layer from bacterial cellulose was developed and a pre-deposited coating was used on the UF membrane surface. The results revealed that permeate flux and the natural organic matter (NOM) removing were improved [26]. Grafting the polyacrylic acid (PAA) on MWCNTs surface by in situ polymerization was done by Daraei et al. [27]. The results showed that water flux and antifouling properties, salt rejection and hydrophilicity of prepared membranes were improved.

The carbon atom naturally has three allotropes: diamond, amorphous carbon and graphite. Of these, graphite is the most stable state under standard conditions. Graphite is a crystalline structure of carbon that is very soft and has very low specific gravity and crushes with the slightest pressure. But it is very resistant to heat and almost neutral to any other materials. This property of graphite has led to a wide range of metallurgical and fabrication applications. Numerous studies have proven that graphite is a special mineral that possesses extraordinary properties such as high heat and electricity conductivity, high natural hardness and high resistance to temperatures [28-30].

Graphite is a three-dimensional carbon allotrope of a layered structure in which the four-valent carbon atoms are bonded to three other carbon atoms via three covalent bonds and form a hexagonal lattice structure. Each of these layers is called a graphene sheet or layer. Each sheet is parallel to the other sheet and generates a regular grid. Thus, the fourth electron capacity also binds the sheets together by making a van der Waals link between the layers. Due to the weak bonds between the graphene sheets (van der Waals bond), the sheets above can easily slide over each other. In Fig. 1,

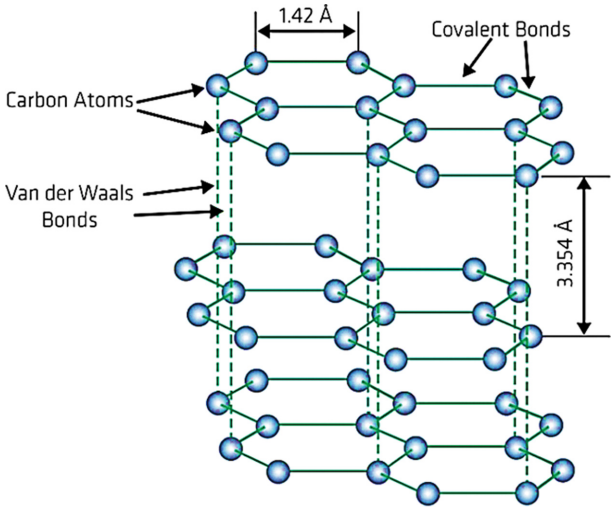

Fig. 1. Three-dimensional grid structure of Graphite [34].

in the three-dimensional grid structure of graphite, the distance between the carbon atoms is 14.2 Å (0.142 nm) and the distance between the graphene sheets is about 3.354 Å (0.335 nm) [31]. Nano-sized graphite has superior properties such as stronger adsorption, easier dispersion and higher surface activity than graphite samples with micron-sized or more. Nano-graphite has excellent properties such as high surface area, good lubrication, special conductivity properties, good mechanical properties, proper corrosion resistance, high thermal conductivity, low density, higher surface energy, good biocompatibility, and easier and cheaper production than other carbon materials (such as carbon nanotubes, graphene oxide and graphene). For this reason, it is used in many fields such as adsorption, biosensor, and photo electrochemical degradation [32]. Besides, the antibacterial activity of graphite makes it a good candidate in membrane fabrication for water treatment.

In the present work, the effect of incorporating of graphite nanoparticles into PES-based nanofiltration membrane was studied. Graphite nanoparticles are known to be hydrophobic, and their use in nanofiltration membranes for water purification applications is not common. But given the special properties already mentioned for graphite, it is expected that this structural modification can improve their separation, antifouling and antibacterial performance. The graphite nanoparticles were added to the membrane structure by the blending method.

MATERIALS AND METHODS

1. Materials

Polyethersulfone (PES Ultrason E6020P, MW=58,000 g/mol), polyvinylpyrrolidone (PVP, Merck, MW: 25,000 g/mol), N, N, dimethyl acetamide (DMAc, Merck, Mw: 87.12 g/mol), graphite nanoparticles (G, US NANO Company, 400 nm average particle size, 99.9% purity), Sodium Sulfate (Na_2SO_4, Merck, Mw: 142.04 g/mol) and deionized water.

2. Preparation of Membranes

All the membranes were prepared during the phase inversion method. PES, PVP, DMAc and different concentration of graphite

Table 1. The composition of the polymer solution used to make the membranes

Sample	Membranes	PES (wt%)	PVP (wt%)	DMAc (wt%)	Graphite nanoparticles (wt%)
1	M0	18	1	81.00	0.00
2	M1	18	1	80.95	0.05
3	M2	18	1	80.90	0.10
4	M3	18	1	80.50	0.50
5	M4	18	1	80.00	1.00

nanoparticles was combinations of casting solutions. Table 1 represents the polymeric solution compositions. The polymeric solutions were stirred by mechanical stirrer at 350 rpm (model: Velp Scientifica Multi 6 stirrer). Afterward, for good dispersing and breaking up agglomeration of nanoparticles, samples were placed in an ultrasonic bath for 1 hr (Parsonic11Smodel, S/N PN-88159, and Iran). For removing the air bubbles completely, the prepared solutions were kept at room temperature for one day. After that, the homogeneous solutions were cast by a casting knife with 150 μm thickness on clean glass plates. The precipitation process involved immersing the prepared films in a non-solvent bath (deionized water). To remove the extra solvent, the prepared membranes were washed and kept in water for at least one day. Subsequently, the membranes were kept between two sheets of paper for one day. All procedures were performed at 25 °C.

3. Scanning Electron Microscopy (SEM)

To study the internal structure of fabricated membranes using cross-sectional images, small samples of membranes were prepared, and after being stored in liquid nitrogen for 15 min they were broken. After this step, samples were covered with gold-coated for microscope imaging.

4. Scanning Optical Microscopy (SOM) and 3D Surface Image

The membrane surface changes in terms of the distribution of nanoparticles were investigated using scanning optical microscopy. Images were taken from specimens of membranes cut between two glass plates. Also, the images obtained from SOM were evaluated with FemtoScan software to produce 3D surface images for surface roughness calculations and analysis.

5. Water Content and Contact Angle Studies

To calculate the water content, the same size samples were prepared from membranes and stored in deionized water for 24 hours under ambient conditions. The samples were then brought out from the water and placed between two sheets of filter paper to remove excess water from the membrane surface. The weight of the samples was measured immediately; the specimens were then placed in an oven for four hours at 60 °C to calculate their weight after measurement. These steps were performed three times for each sample and their averages were reported to minimize measurement error. Eq. (1) is used to calculate this parameter [14,35]:

$$\%\text{Water content} = \frac{w_w - w_d}{w_w} \times 100 \quad (1)$$

where w_w and w_d are the weight of wet and dried membranes, respectively. Since membrane hydrophilicity is very important in water purification processes, the contact angle analysis of water at the surface of the membrane was prepared. Three random points from each sample of membranes were examined for contact angle analysis and the mean of measurements was declared as the final number. All samples were tested under ambient conditions with deionized water as probe liquid.

6. Porosity and Mean Pore Radius

The membrane porosity is calculated by the following formula [36]:

$$\varepsilon(\%) = \left(\frac{w_{wet} - w_{dry}}{A \times l \times d_w}\right) \times 100 \quad (2)$$

where ε is the membrane porosity; w_w and w_d are the same as the values mentioned earlier. A is the effective membrane surface area (m), d_w represents the water density (kg/m^3) and l is the thickness of the membranes sample. Porosity measurements have also been reported on the average of three times measurements, to reduce the error.

The Guerout-Elford-Ferry Eq. (3) is used to calculate the mean radius of the pores assuming the pores are cylindrical. This equation is based on pure water flux [36].

$$r_m = \sqrt{\frac{(2.9 - 1.75\varepsilon) 8 \eta l Q}{\varepsilon \times A \times \Delta P}} \quad (3)$$

Such that ε is the membrane porosity, η is the water viscosity (8.9×10^{-4} Pa·s), l is the membrane thickness (m), Q refers to the pure water flux (m^3/s), and ΔP is the operating pressure (5 bar).

7. Mechanical Characterization

The mechanical tensile strength study was applied (ASTM-1922) to evaluate the effect of graphite nanoparticles on the mechanical behavior of prepared membranes [37]. For the aim, membranes were cut into small sizes and the maximum tolerable load of membranes was reported. Measurements were performed three times for each sample and the mean average value reported.

8. Flux and Salt Rejection

In the evaluation of membrane separation performance, two parameters of rejection and flux are particularly important. The nanofiltration dead-end cell was used to obtain these two parameters (Fig. 2); the cell has an agitator to delay the polarization process. The driving force of the system is the pressure of 5 bar, supplied by the nitrogen gas capsule. The membrane crossing flux is calculated by the following equation [14].

$$J = \left(\frac{V}{A \times \Delta t}\right) \quad (4)$$

where J is permeation flux (l/m^{2}h), V is the content of permeated water (l); A refers to membrane area (m^2) and Δt shows sampling time (h). All experiments were done at ambient temperature.

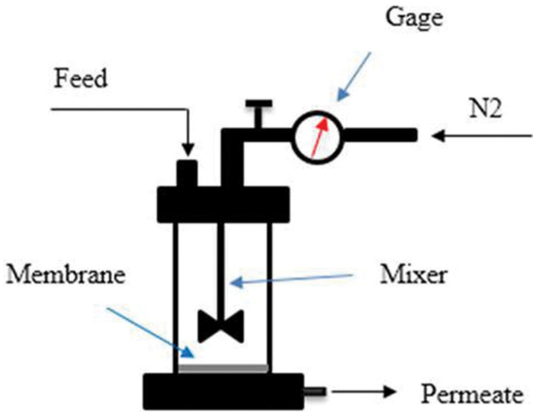

Fig. 2. Schematic diagram of nanofiltration dead-end cell.

Membrane separation efficiency is calculated by Eq. (5). The feed solution for test is sodium sulfate aqueous solution with a concentration of 0.01 M [35,38].

$$\text{Rejection } \% = 1 - \left(\frac{C_p}{C_f}\right) * 100 \quad (5)$$

where C_p is the concentration of permeate solution and C_f is the concentration of feed solution and both of them were measured by a conductivity meter.

9. Investigation the Antifouling Ability of Prepared Membranes

To evaluate the anti-fouling properties of the membranes, a protein solution is used. The protein solution is a solution of milk powder with a concentration of 8,000 mg/L. The antifouling property is also specified by the flux recovery ratio (FRR) parameter. For this purpose, first, pure water flux, $J_{W,1}$, was measured for 1.5 hours at the pressure of 5 bar. The membranes then were tested with a protein solution at the same pressure and duration and term J_P was obtained. Due to the accumulation of protein particles, the polarization phenomenon is unavoidable at this stage. The foulant membranes were immersed in deionized water for one hour to reduce the fouling. Finally, the pure water flux for the washed membrane was re-measured under the same conditions (5 bar and 1.5 h) to achieve $J_{W,2}$. Eventually, the value of the flux recovery ratio (FRR) was calculated by the following equation [39]:

$$FRR = (J_{w,2}/J_{w,1}) * 100 \quad (6)$$

The fouling phenomenon in the membrane, which is defined by

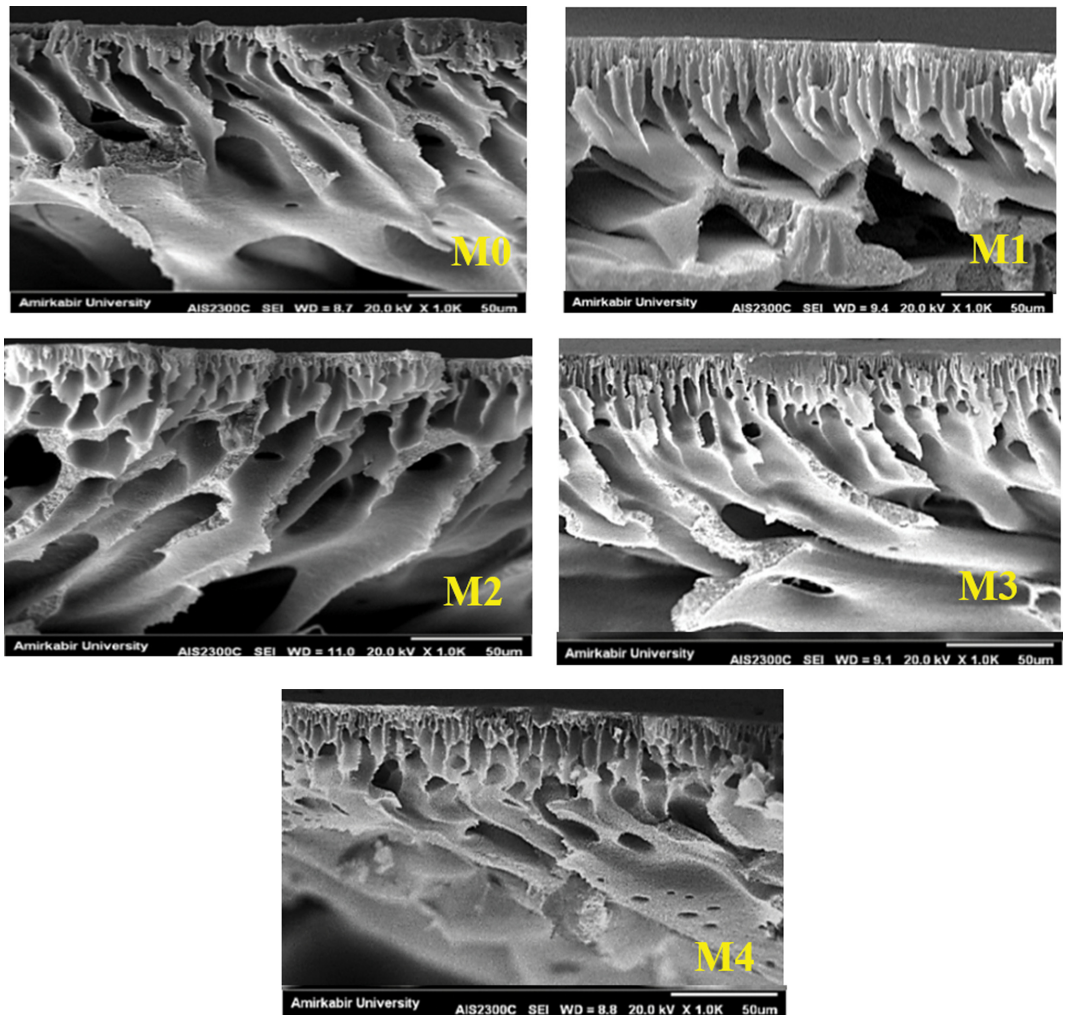

Fig. 3. SEM images of prepared membranes with different concentration of graphite nanoparticles.

the R_p, is caused by the formation of a cake layer on the surface of the membrane and the absorption of foulant on the surface or inside the pores of membrane. This parameter itself contains two types of fouling: reversible, which has poor bonding with the membrane and is removable, and non-reversible, which stays in the membrane and reduces the flow rate and weakens the membrane function. The calculations of these three factors, reversible fouling ratio (R_r), irreversible fouling ratio (R_{ir}) and total fouling (R_t) are given as following equations [39]:

$$Rt = \left(1 - \frac{J_p}{J_{w,1}}\right) \times 100 \quad (7)$$

$$Rr = \left(\frac{J_{w,2} - J_p}{J_{w,1}}\right) \times 100 \quad (8)$$

$$Rir = \left(\frac{J_{w,1} - J_{w,2}}{J_{w,1}}\right) \times 100 \quad (9)$$

10. Antimicrobial Activity of Mixed Matrix Membrane

The viability/growing of E. coli in presence of membranes were considered during 4 h for the aim. All measurements were repeated three times to minimize the experimental error.

RESULTS AND DISCUSSION

1. Membrane Morphology

The SEM images represent the cross-sectional structure of the membranes (Fig. 3). In the picture below, all membrane samples have an asymmetric, two-layer structure. The active layer is a thin but dense layer that plays the major role in separation. The sublayer part is that thick but porous layer, with a supporting role; in fact, this section has channels for passing the liquid. As shown in the pictures, the inner structure of the membranes has become cylindrical (finger-like) with the addition of nanoparticles. The number and size of pores also increased in membranes containing nanoparticles and bigger channels and macro-voids have been produced. As is clear in Fig. 4, though graphite nanoparticles are hydrophobic, due to their lightness and low density, they move to the surface of the membrane and interface area; this is quite clear from the color difference between the surface and the back of the membrane. Movement of nanoparticles to the surface of the membranes creates a smooth surface that enhances the exchange rate between solvent (DMAc) and non-solvent (water). This event accelerates the mass transfer of non-solvent (water) through the membrane and increases the deposition rate of PES during membrane formation, resulting in phase separation instantly; as the phase change speed increases, more channels and cavities are formed [40,41]. In fact, as shown in Fig. 4, the membrane structure resembles a double-layer membrane: the top layer is rich in graphite nanoparticles and the bottom layer is rich in polyether sulfone polymer.

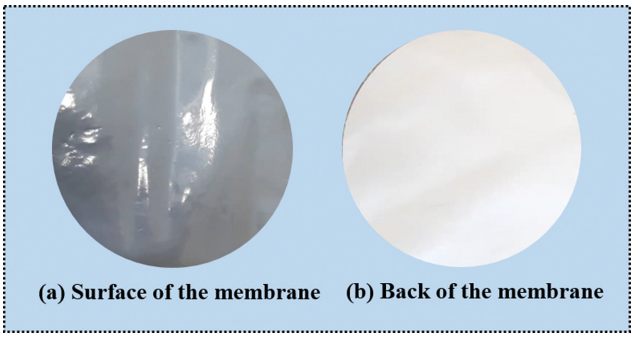

Fig. 4. A typical image of surface and back of prepared PES-graphite membrane (M3).

However, with increasing nanoparticle percentage and increasing polymer solution concentration, the nanoparticles become more clogged and aggregated, which reduces the rate of phase change. For this reason, at higher percentages of nanoparticles, the structure of membranes becomes denser and the porosity of the membranes diminishes; also closed-end channels and fewer cavities are formed in the membrane structure [39].

Fig. 5 presents the SOM images of the fabricated membranes. These images are intended to show how nanoparticles are distributed in the membrane. It is clear that the nanoparticles are homogeneously and uniformly dispersed throughout the membrane surface. Proper distribution of the nanoparticles reduces clumping and aggregation, thus making them more efficient.

In the following, with the help of SOM images and using the Fem to scan software, surface roughness analysis of the membranes was also performed (Fig. 5). The roughness parameter is the benchmark for measuring the hydrophilicity of the membranes. In fact, a membrane with the lower surface roughness is more hydrophilic and a membrane with a rougher surface is less hydrophilic. Membrane surface roughness images have concavity and convexity. The dark points show the concavity and the light points show the convexity. Adding nanoparticles to the polymer solution by changing the membrane surface morphology causes some changes in surface roughness. M1 shows rougher surface than the base membrane. As mentioned earlier, the movement of nanoparticles to the membrane surface due to the lower density and particle placement in the concave regions reduces the surface roughness of the membrane and the surface becomes smoother. But further, by adding more nanoparticles, there is an upward trend. This is due to the accumulation of nanoparticles on the membrane surface, which intensifies the concavity and convexity of the membrane surface, so that the roughness value for samples M2, M3 and M4 is greater than the virgin sample [42].

2. Porosity and Water Content

It is quite obvious that the two parameters of porosity and the water content are directly related to each other. Fig. 6 shows the changes of these two agents due to the addition of graphite nanoparticles to the membrane structure. As shown in the following diagram (Fig. 6), the porosity and water content of all the modified membranes is higher than that of the nanoparticle-free membrane. The reason may be related to the specific properties of graphite nanoparticles. In fact, when nanoparticles due to their low density are transferred to the polymer solution and non-solvent (water) interface, and also because of their high energy level, they interact more rapidly with the solvent than the polyether sulfone polymer. This creates cavities and pores at the membrane surface and channels in the inner structure of the membranes. Also, due to the presence of nanoparticles in the polymer solution, the bonds between

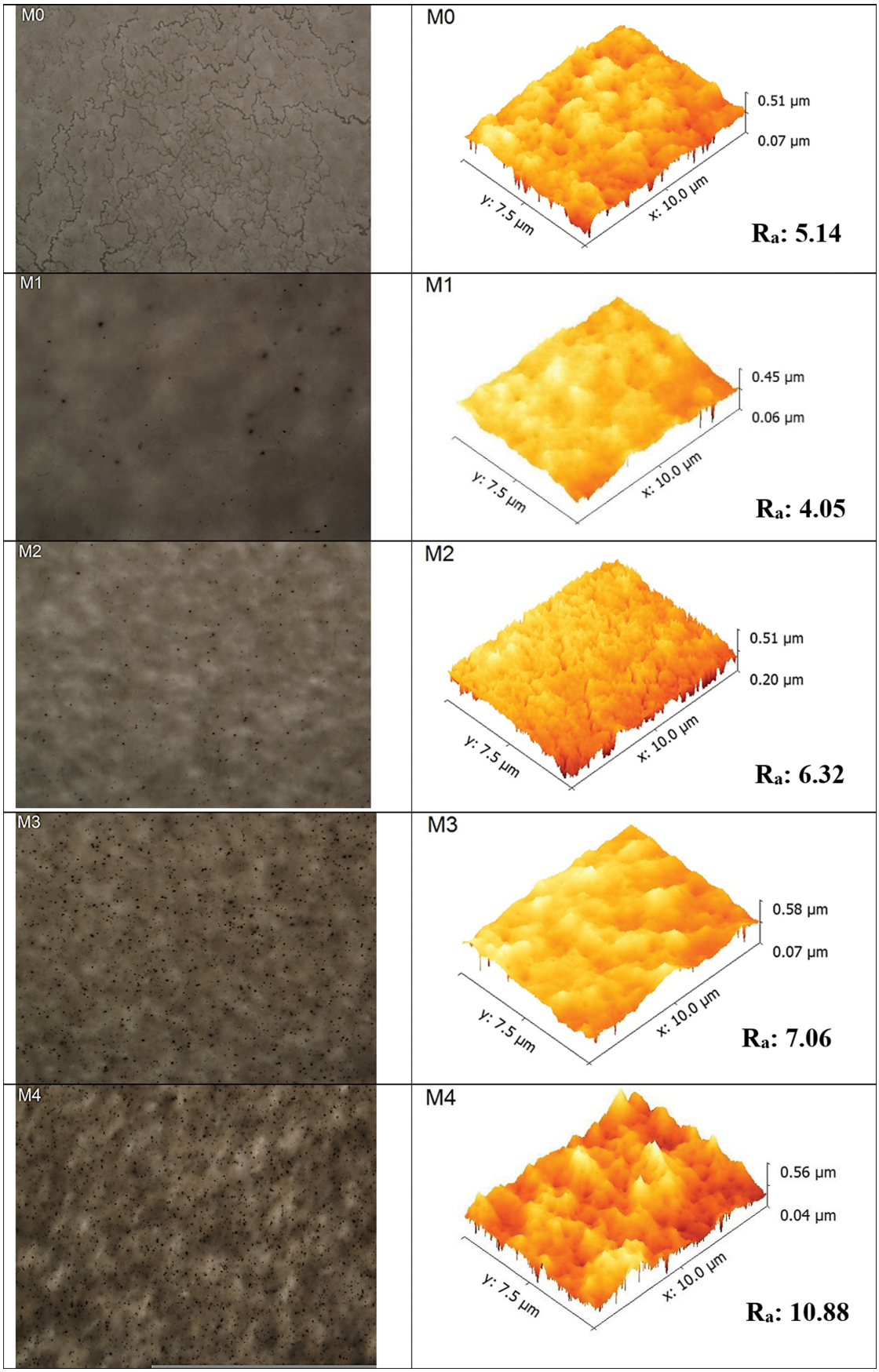

Fig. 5. SOM images, 3D images and surface roughness of membranes: M0, M1, M2, M3 and M4.

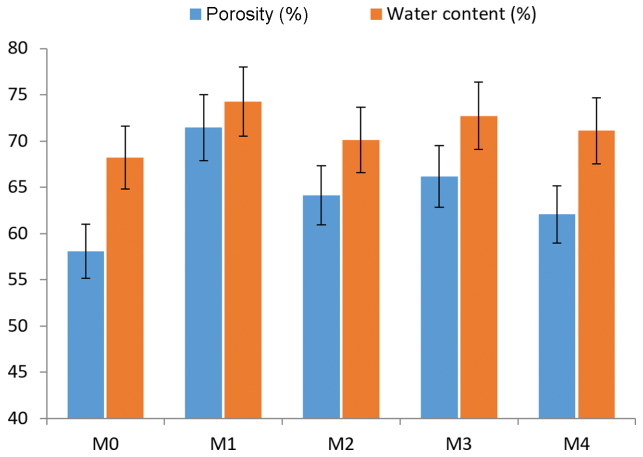

Fig. 6. The effect of graphite nanoparticle content on porosity and water content.

the polymer chains are weakened and this creates more voids in the membrane, which increases the porosity and therefore the amount of water stored inside the channels, cavities and voids in the membrane [39].

As the percentage of graphite in the membrane structure increases, due to the accumulation of nanoparticles and their agglomeration, their active surface area decreases and so the exchanges with water reduced and nanoparticles become trapped in cavities and channels, closing the pores and eventually reducing the porosity and water content. However, the porosity and water content of the modified membrane with a high percentage of nanoparticles are still higher than the base membrane. As can be seen from the results, the changing trend of both parameters is quite consistent [14].

3. Water Contact Angle

One of the important properties of the membrane against fouling is the membrane hydrophilicity. The hydrophilic property actually shows how the water molecule interacts with the membrane surface. The surface functionality and roughness are the main parameters that affect surface hydrophilicity. A membrane with the rougher surface is more hydrophobic and, conversely, a membrane with a smoother surface is more hydrophilic. As shown in Table 2, the water contact angle was reduced initially by use of graphite nanoparticles in membrane matrix. This may be assigned to smoother surface for M1 that produce more hydrophilic surface for this sample. The water contact angle was increased again by more increase of graphite ratios in the membrane body for M2 to M4. This may be due to increase of surface roughness and hydrophobic nature of graphite nanoparticles that provide more hydrophobic surface for them.

Table 2. The Water contact angle for prepared membranes

Samples	Water contact angle (°)
M0	79.46±1.2
M1	66.34±1.4
M2	74.05±2.1
M3	75.18±1.5
M4	81.44±1.8

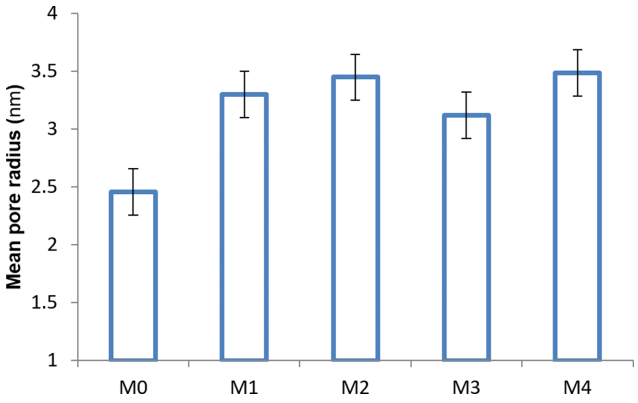

Fig. 7. The effect of graphite ratios on membrane mean pore radius.

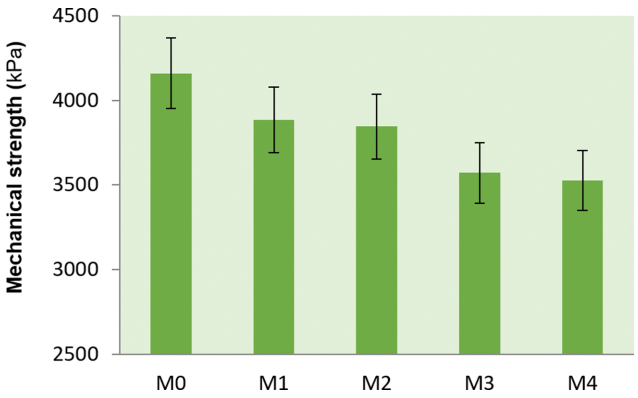

Fig. 8. The mechanical strength behavior of membranes.

4. Mean Pore Radius Measurement

According to Fig. 7, all modified membranes have larger pores than M0. This may be due to increase of membrane heterogeneity assigned to presence of graphite nanoparticles. Moreover, the high surface energy and good dispersibility in the membrane structure could change the exchange rate of polymer solution with water molecules during phase change that creates pores with greater diameter [43].

5. Mechanical Characterization

According to Fig. 8, the mechanical strength of the modified membranes decreased compared to the base membrane. This could be due to the increase in the size of the cavities, the increase in the number of channels and vacancy in the membrane structure. In fact, the structure of the membrane is loosened and the polymer chain bonds have been reduced due to the presence of graphite nanoparticles and decreased membrane stiffness. On the other hand, because graphite has a layered structure and is very soft, it breaks down at the slightest pressure, so the higher the percentage of graphite in the membrane, causing the lower mechanical strength. But in the meantime, sample M1 had better resistance than other nanoparticle-containing membranes.

6. Flux and Salt Rejection

Two noteworthy factors in discussing membrane performance

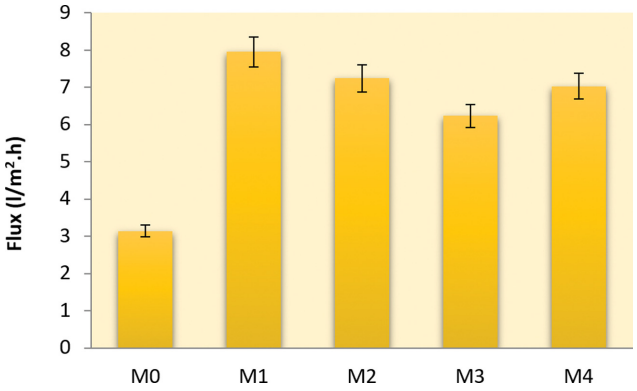

Fig. 9. The flux change trend with increasing graphite nanoparticles.

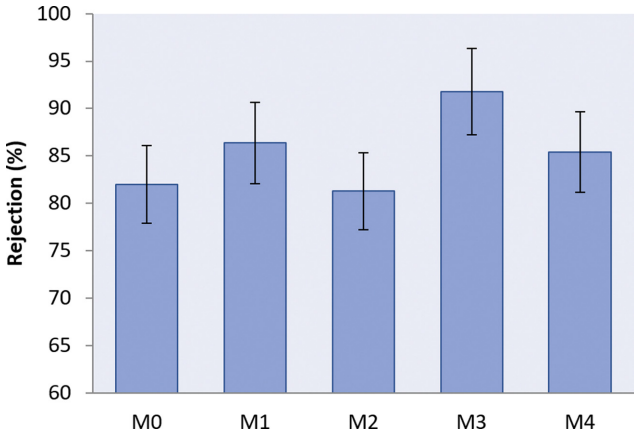

Fig. 10. The salt rejection of prepared membranes.

evaluation are separation efficiency and flux rate. Based on what is shown in Fig. 9, the flux was significantly increased for all samples containing nanoparticles. Factors that can justify this process include increasing porosity, increasing the number and size of channels and membrane pores, decreasing the contact angle and decreasing the active layer thickness. However, graphite nanoparticles have the ability to be channelized due to their layered structure (Fig. 1) and can provide pathways for water. Of course, among the modified samples, M1 had the highest flux increase (more than 2.5 times that of the base membrane) because, at low percentages of nanoparticles, the probability of aggregation was lower, distribution was better, active sites were free and the surface energy was more. Since the surface of the M1 membrane is smoother, the water molecules are easier to attach to the surface of the membrane and pass through the pores and enter the inner structure of the membrane in the form of finger-like channels and, due to the higher porosity of the membrane, pass faster. At higher percentages due to the accumulation of nanoparticles, the active sites are involved, the surface energy of the nanoparticles is reduced and the performance of graphite nanoparticles is impaired. Due to the accumulation of nanoparticles, the membrane surface becomes rougher and acts as a barrier for the penetration of water molecules into the pores. On the other hand, because the porosity of the membrane is reduced due to the blocking of the pores by the nanoparticles, the water passages are limited and the flux rate is lower compared to sample M1. In M4 sample, due to the weak connections and the destruction of the channel walls and their connection to each other, the flux has increased again.

As mentioned, one of the important parameters in membrane separation is rejection. Fig. 10 presents the data obtained for rejection. The membrane rejection was increased initially by incorporating filler nanoparticles in membrane matrix which can be assigned to the unique structure and adsorption property of graphite nanoparticles. As shown Fig. 1, the graphite structure is in the form of layers with a certain distance, each layer having its own network structure. Therefore, the efficiency is expected to improve somewhat. Of course, the separation mechanism is influenced by the presence of graphite nanoparticles in the form of molecular sieving, which is mainly dominated by interlayer sieving [44]. As the distance between the layers in the nano graphite is 0.335 nm and the mean ion-water inter-nuclear distance of the sulfate ion is 0.381 nm, therefore, the size of the hydrated sulfate ions is greater than the distance between the graphite layers and this increases their rejection via interlayer sieving mechanism [45]. Although hexagonal network connection of carbons in graphite can also act as a trap for capturing salt ions. In addition, the high adsorption behavior of graphite should not be forgotten, which can be a factor in increasing separation performance. Decrease of salt rejection for M2 may be also assigned to bigger mean pore size for this sample that facilitates the salt ions percolation through the membrane. Moreover, decline in salt rejection for M4 at 1%wt graphite loading ratio may be due to nanoparticle agglomeration at high additive concentration that is beneath their adsorption capacity as well as crack propagation in membrane matrix. This would decline the rejection accordingly.

Among the modified samples, M3, with 91.79% efficiency and sample M1, with 86.36% efficiency, performed well in separation. However, since efficiency and flux are considered as two separation parameters, both factors must have acceptable values. Since sample M2 has less flux than sample M1, sample M1 with flux ~7.95 and rejection ~86.36% were considered as the optimal membrane.

Moreover, to study the flux stability of prepared membranes, their permeability was considered during time. Decreasing flux ratio measured <20% for the mixed matrix membranes, whereas that was >45% for the virgin membrane after one-and-a half hour filtration.

7. Antifouling Performance

To determine the antifouling property, the optimal membrane (M1) and the nanoparticle-free membrane (M0) were investigated. The protein solution was used for this experiment. First, the pure water flux ($j_{w,1}$) was measured, then the protein solution flux (milk powder solution, j_p), and finally, the pure water flux ($j_{w,2}$) was evaluated again after washing the membranes. All three values and their variations in both samples are clearly shown in Fig. 11. It is obvious that the milk powder test has a large flux reduction compared to the primary pure water, due to the presence of protein particles at the membrane surface or inside the pores and channels, which caused clogging and blocking the passage of flow. After that, the pure water re-test had a higher flux value but not as much as the first step. The difference between the pure water flux before and after the milk powder test shows the membrane's ability

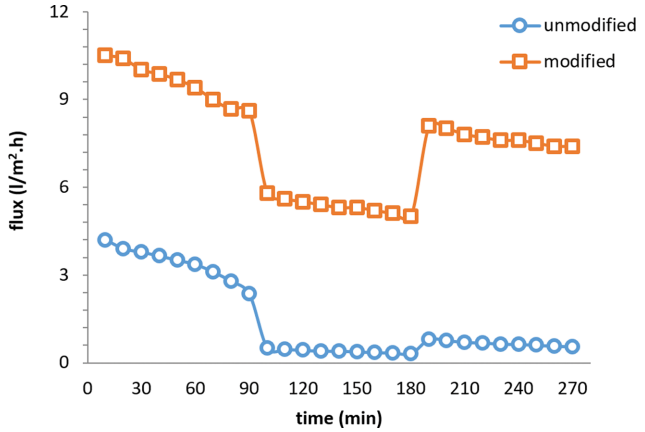

Fig. 11. The $j_{w,1}$, j_p and $j_{w,2}$ of virgin membrane (M0) and M1 as optimum membrane.

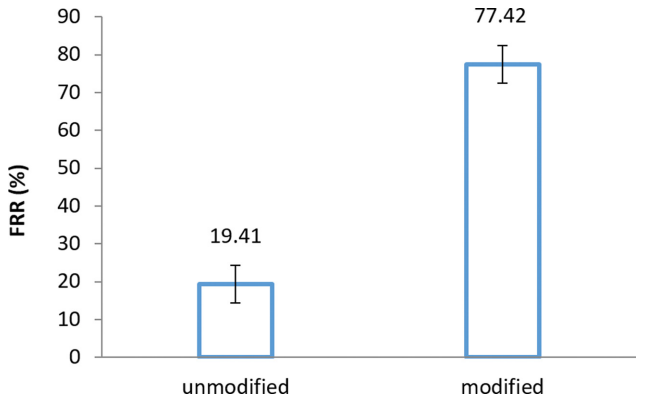

Fig. 12. The FRR Parameter for M0 and M1.

to be fouled. The greater difference means the lower membrane's antifouling performance. Of course, this difference is calculated by factor FRR that is provided in Fig. 12.

Indicator FRR had a significant value for the modified membrane with 0.05 wt% graphite nanoparticles. This is related to lower surface roughness and smaller water contact angle, which increases the hydrophilicity of the membrane. By increasing the hydrophilicity at the surface, the membrane surface interactions with the water molecules increase and the water molecules form a layer on the membrane surface that also acts as a barrier against the protein particles and decreases the adsorption of these particles on the surface. Also, more movement of water molecules on the surface of the membrane causes the surface to be washed away by undesirable particles, and the phenomenon of fouling occurs later [46].

As illustrated in Fig. 13, fouling has two reversible and irreversible parts. The reversible part (R_r) incorporates loose joints that are remedied by simple hydraulic methods, but the irreversible part (R_{ir}) has made stronger connections to the membrane structure and can be remedied by chemical methods that increase cost and energy consumption; it also reduces the life of the membrane. The total fouling (R_t), which is the sum of reversible and irreversible fouling, is lower in the modified sample (M1) and most of it is reversible fouling.

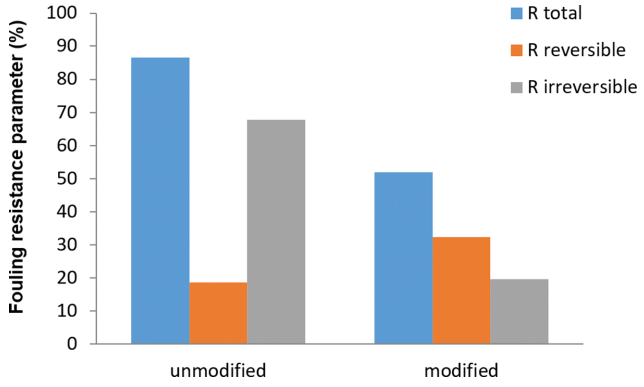

Fig. 13. The values of fouling factors for modified (M1) and unmodified (M0) membranes.

8. Antibacterial Ability Study

The viability of Escherichia-coli bacteria in the presence of prepared membranes was studied. Three cells, including control, M0 plus E-coli, and graphite-PES blended membrane with E-coli were prepared. Results exhibited >23% cell inactivation for the sample containing blended membrane compared to control, whereas that was inconsiderable for the sample with pristine membrane. This may be ascribed to stress on bacterial cells as well as oxidative stress mechanism toward neural cells [47].

CONCLUSION

Graphite nanoparticles were evaluated to improve the performance of polyethersophone nanofiltration membranes. Due to the hydrophobicity of these nanoparticles, the increased hydrophilicity of the membranes was a little unexpected, but based on experiments and observations, interesting results were obtained. The use of graphite nanoparticles in small quantities reduced the surface roughness of the membrane and increased the hydrophilicity of the membrane by reducing the contact angle at the membrane surface. So that the water flux increased by about 2.5 times compared to the unmodified membrane. Separation efficiency also increased. More important was the enhancement of the antifouling property, which increased from 19.41 for the base membrane to 77.42 for the modified membrane; it increased almost four times. Moreover, blended membranes showed antibacterial activity against E-coli.

REFERENCES

1. A. Kalfa, B. Shapira, A. Shopin, I. Cohen, E. Avraham and D. Aurbach, *Chemosphere*, **241**, 125003 (2020).
2. T. A. Makhetha and R. M. Moutloalia, *J. Membr. Sci.*, **554**, 195 (2018).
3. S. Wu, Y. Ge, Y. Wang, X. Chen, F. Li, H. Xuan and X. Li, *Environ. Technol.*, **39**, 1937 (2018).
4. C. Zhao, J. Xue, F. Ran and S. Sun, *Prog. Mater. Sci.*, **58**, 76 (2013).
5. D. M. Davenport, J. Lee and M. Elimelech, *Sep. Purif. Technol.*, **189**, 389 (2017).
6. W. Jiang, Y. Wei, X. Gao, C. Gao and Y. Wang, *Desalination*, **359**, 26 (2015).

7. N. Nasrollahi, S. Aber, V. Vatanpour and N. M. Mahmoodi, *Mater. Chem. Phys*., **222**, 338 (2018).
8. Z. Kiamehr, B. Farokhi and S. M. Hosseini, *Korean J. Chem. Eng*., **38**, 114 (2021).
9. N. Nasrollahi, V. Vatanpour, S. Aber and N. M. Mahmoodi, *Sep. Purif. Technol*., **192**, 369 (2017).
10. T. D. Dipheko, K. P. Matabola, K. Kotlhao, R. M. Moutloali and M. Klink, *Int. J. Polym. Sci*., **1**, 3587019 (2017).
11. F. Gholami, S. Zinadini, A. A. Zinatizadeh and A. R. Abbasi, *Sep. Purif. Technol*., **194**, 272 (2017).
12. L. Gzara, Z. A. Rehan, S. Bahadar Khan, K. A. Alamry, M. H. Albeirutty, M. S. El-Shahawi, M. Imtiaz Rashid, A. Figoli, E. Drioli and A. M. Asiri, *J. Taiwan Inst. Chem. Eng*., **65**, 405 (2016).
13. H. Rajabi, N. Ghaemi, S. S. Madaeni, P. Daraei, B. Astinchap, S. Zinadini and S. H. Razavizadeh, *Appl. Surf. Sci*., **349**, 66 (2015).
14. F. Halek, S. Koudzari Farahani and S. M. Hosseini, *Korean J. Chem. Eng*., **33**, 629 (2016).
15. A. L. Ahmad, A. A. Abdulkarim, Z. M. H. Mohd Shafie and B. S. Ooi, *Desalination*, **403**, 53 (2016).
16. O. T. Mahlangu, R. Nackaerts, J. M. Thwala, B. B. Mamba and A. R. D. Verliefde, *J. Membr. Sci*., **524**, 43 (2017).
17. Y. L. Ji, W. J. Qian, Y. W. Yu, Q. F. An, L. F. Liu, Y. Zhou and C. J. Gao, *Chin. J. Chem. Eng*., **25**, 1639 (2017).
18. M. Rabbani Esfahani, S. Aghapour Aktij, Z. Dabaghian, M. Dadashi Firouzjaei, A. Rahimpour, J. Eke, I. C. Escobar, M. Abolhassani, L. F. Greenlee, A. R. Esfahani, A. Sadmani and N. Koutahzadeh, *Sep. Purif. Technol*., **213**, 465, (2019).
19. D. M. Davenport, J. Lee and M. Elimelech, *Sep. Purif. Technol*., **189**, 389 (2017).
20. P. Kumari, M. Alam and W. A. Siddiqi, *Sustain. Mater. Technol*., **22**, e00128 (2019).
21. X. Fan, Y. Liu and X. Quan, *Desalination*, **451**, 117 (2019).
22. S. Gholami, J. López, A. Rezvani, V. Vatanpour and J. L. Cortina, *Chem. Eng. J*., **384**, 123348 (2020).
23. Y. Li, S. Shi, H. Cao, Z. Zhao, C. Su and H. Wen, *J. Membr. Sci*., **566**, 44 (2018).
24. G. Yang, Z. Xie, M. Cran, D. Ng and S. Gray, *J. Membr. Sci*., **579**, 40 (2019).
25. M. H. Tai, J. Juay, D. D. Sun and J. O. Leckie, *Sep. Purif. Technol*., **156**, 952 (2015).
26. T. Liua, H. Zhoua, N. Grahamb, Y. Liana, W. Yub and K. Suna, *J. Membr. Sci*., **557**, 87 (2018).
27. P. Daraei, S. S. Madaeni, N. Ghaemi, H. Ahmadi Monfared and M. A. Khadivi, *Sep. Purif. Technol*., **104**, 32 (2013).
28. M. Ali Raza, A. Westwood, A. Brown, N. Hondow and C. Stirling, *Carbon*, **49**, 4269 (2011).
29. G. Sun, X. Li, Y. Qu, X. Wang, H. Yan and Y. Zhang, *Mater. Lett*., **62**, 703 (2008).
30. A. Barak, V. D. Gangwar and S. K. Shukla, *Ind. J. Chem. Technol*., **25**, 196 (2018).
31. S. Stankovich, D. A. Dikin, G. H. B. Dommett, K. M. Kohlhaas, E. J. Zimney, E. A. Stach, R. D. Piner, S. T. Nguyen and R. S. Ruoff, *Nature*, **442**, 282, (2006).
32. H. Ke, *Sol. Energy*, **173**, 1197 (2018).
33. S. H. M. Akhair, Z. Harun, H. Basric, R. A. R. Ahmad, A. Q. A. Rashid and F. H. Azhar, *Inter. J. Eng*., **31**, 1381 (2018).
34. http://www.substech.com.
35. S. Koudzari Farahani, F. Halek and S. M. Hosseini, *Korean J. Chem. Eng*., **32**, 2097 (2015).
36. V. Vatanpour, S. S. Madaeni, R. Moradian, S. Zinadini and B. Astinchap, *Sep. Purif. Technol*., **90**, 69 (2012).
37. E. Bagheripour, A. R. Moghadassi, F. Parvizia and S. M. Hossein, *Chem. Eng. Res. Des*., **144**, 418 (2019).
38. R. Khan, F. Shen, K. Khan, L. X. Liu, H. H. Wu, J. Q. Luo and Y. H. Wan, *RSC Adv*., **6**, 28895 (2016).
39. F. Zareei and S. Mohsen Hosseini, *Sep. Purif. Technol*., **226**, 48 (2019).
40. P. Daraei, S. S. Madaeni, N. Ghaemi, E. Salehi, M. Khadivi, R. Moradian and B. Astinchap, *J. Membr. Sci*., **415**, 250 (2012).
41. X. Chang, Z. Wang, S. Quan, Y. Xu, Z. Jiang and L. Shao, *Appl. Surf. Sci*., **316**, 537 (2014).
42. M. Moochani, A. R. Moghadassi, S. M. Hosseini, E. Bagheripour and F. Parvizian, *Korean J. Chem. Eng*., **33**, 2674 (2016).
43. F. Zareei, S. Bandehali and S. M. Hosseini, *Korean J. Chem. Eng*., **38**, 1014 (2021).
44. S. J. Fishlock, S. H. Pu, G. Bhattacharya, Y. Han, J. Mc Laughlin, J. W. Mc Bride, H. M. H. Chong and S. J. O'Shea, *Carbon*, **138**, 125 (2018).
45. Y. Marcus, *Chem. Rev*., **88**, 1475 (1988).
46. H. Koulivand, A. Shahbazi and V. Vatanpour, *Chem. Eng. Res. Des*., **145**, 64 (2019).
47. S. Liu, T. H. Zeng, M. Hofmann, E. Burcombe, J. Wei, R. Jiang, J. Kong and Y. Chen, *ACS Nano*, **5**, 6971 (2011).